Interface modification of the InGaN/GaN quantum wells: the strain pre-relief effect

2009 Nanotechnology 20 235401

(http://iopscience.iop.org/0957-4484/20/23/235401)

Nanotechnology **20** (2009) 235401 (7pp) doi:10.1088/0957-4484/20/23/235401

Interface modification of the InGaN/GaN quantum wells: the strain pre-relief effect

Z L Fang[1,3], D Q Lin[1], J Y Kang[1], J F Kong[2] and W Z Shen[2]

[1] Semiconductor Photonics Research Center, Department of Physics, Xiamen University, Xiamen 361005, People's Republic of China
[2] Department of Physics, Shanghai Jiao Tong University, Shanghai 200030, People's Republic of China

E-mail: zhilaifang@hotmail.com

Received 24 January 2009, in final form 9 March 2009
Published 18 May 2009
Online at stacks.iop.org/Nano/20/235401

Abstract

Interface modification by inserting an ultrathin low-temperature GaN layer prior to the growth of high-temperature GaN barriers followed by an annealing process was employed to improve the properties of the InGaN/GaN quantum wells. By detailed studies and comparisons of the surface morphology, photoluminescence and the surface compositions of the InGaN/GaN quantum wells at different growth stages with and without the interface modification, we find that with the interface modification the surface morphology was significantly improved with better smoothness, and smaller and shallower pits of lower density compared with that without interface modification; further, the indium aggregation and phase separation were suppressed. The physical phenomena are attributed to the 'strain pre-relief effect' by the formation of quasi-dots (∼20 nm in diameter) prior to temperature ramping and growth of high-temperature GaN barriers. Furthermore, the ultrathin low-temperature GaN layers have a good protection property as confirmed by PL and XPS measurements.

(Some figures in this article are in colour only in the electronic version)

1. Introduction

While InGaN alloys have been widely and intensively studied [1–3], and successfully applied in the fabrication of short-wavelength light-emitting diodes (LEDs) and laser diodes [4–7], the epitaxial growth of high-quality InGaN materials required for high-brightness and reliable device applications, especially for general solid-state lighting applications [8–10], is still a big challenge. As common features of the InGaN materials, InGaN alloy phenomena (e.g. decomposition, indium aggregation, phase separation, etc) and the related surface V-defects (pits) would become more severe for high indium content InGaN, resulting in a significant decrease in quantum efficiency. Additionally, the built-in strain of the InGaN/GaN multiple quantum wells (MQWs) and the polarization effects (quantum confined Stark effect) may also cause a reduction of the quantum efficiency. The epitaxy of layer structures with low threading dislocation density, good interface states (structure, stoichiometry, roughness, strain, etc), and good control of layer thickness and doping has become a prerequisite for commercial applications in high-performance optoelectronic devices.

Great efforts have been made to improve the material quality, and to enhance the indium incorporation efficiency and quantum efficiency of green LEDs by the reduction of pit density, increase of surface/interface qualities and suppressing phase separation/aggregation of high indium content InGaN materials [11–27]. As the indium-rich inclusions and the related pits would cause loss of interface abruptness and reduce the device quality, several techniques have been developed towards suppression of embedded inclusions, e.g. with GaN barrier growth either at an elevated temperature or in the presence of hydrogen [28–32]. Recently, surface modification of the GaN films has also been successfully applied for improvement of the subsequently grown InGaN/GaN single quantum well (SQW) [23]. Further, the surface/interface properties (density of indium-rich InGaN nanostructures and surface pits, surface roughness, etc) of the InGaN well layers may also influence the growth behavior of the top GaN barriers and the optical properties of the InGaN/GaN QWs.

[3] Author to whom any correspondence should be addressed.

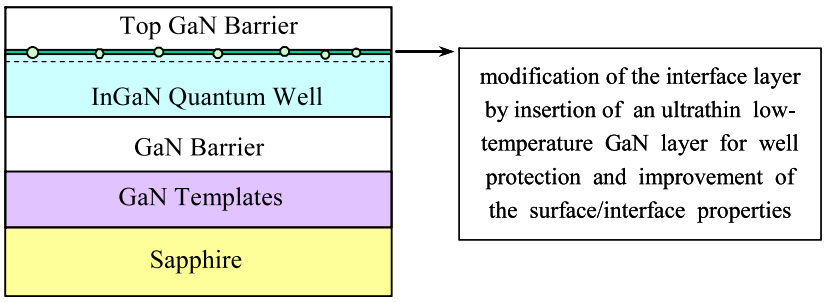

Figure 1. Layer structure of the interface-modified InGaN/GaN SQW on GaN templates.

For example, during the GaN barrier epitaxy the continuous growth of the indium-rich clusters nucleated at the InGaN surface/interface and the enlargement of the InGaN surface pits would increase the pit density and further deteriorate the surface/interface abruptness of the InGaN/GaN MQWs. Accordingly, improvement of the InGaN-to-GaN interface quality would be desirable for the subsequent growth of InGaN/GaN MQWs and the device quality. Recently interface modification by insertion of a low-temperature (LT) GaN layer (about 3–5 nm) between the InGaN well and the GaN barrier has been employed for suppressing the indium loss during the temperature ramping and high-temperature (HT) growth of GaN barriers [24–27].

In the present study, we employed an interface modification technique by insertion of an ultrathin LT GaN layer (about 5–8 Å) between the InGaN wells and the GaN barriers for partial strain pre-relaxation followed by an annealing process. An ultrathin LT GaN layer was employed to avoid the generation of high-density defects during the growth of 'thick' GaN layers at low temperature. The subsequent annealing process was employed for reduction of newly formed defects. By detailed investigation, comparison and analysis of the surface morphology changes, photoluminescence and the surface compositions of InGaN/GaN QWs at different growth stages with and without the interface modification, we find that with interface modification the indium separation/aggregation was suppressed; the surface pit size, depth and density was reduced; the surface smoothness was significantly improved; and this is attributed to the 'strain pre-relief effect'.

2. Experimental methods

The epitaxial growth of GaN films and InGaN/GaN QWs was carried out by metal–organic vapor phase epitaxy (MOVPE) on c-sapphire substrates. Trimethylgallium (TMGa), trimethylindium and high-purity ammonia were used as the source precursors and silane as the n-type dopant. The layer structure is schematically drawn in figure 1. The preparation procedure of the GaN films is briefly described below [33]. Firstly the sapphire substrates were cleaned at 1060 °C and 100 Torr for 15 min in H_2 ambient followed by nitridation at 550 °C for 4 min. A conventional 25 nm LT GaN nucleation layer was grown at 535 °C and 500 Torr followed by an HT annealing process. The subsequent growth of ∼2 μm thick GaN epilayers was carried out at 1035 °C and 100 Torr.

Table 1. Sample reference numbers and the growth conditions.

Sample name	SQW or MQW?	Interface modification		Top GaN barrier
		LT GaN layers?	Annealing?	Yes or no?
A1	SQW	No	No	No
A2	SQW	No	Yes	No
A3	SQW	No		Yes, HT
B1	SQW	Yes	No	No
B2	SQW	Yes	Yes	No
B3	SQW	Yes		Yes, HT
B4	MQW	Yes		Yes, HT
C3	SQW	Yes	No	Yes, LT

The GaN film surface was treated with droplet homoepitaxy for improvement of the surface qualities [34].

The MOVPE of the InGaN/GaN QWs was carried out on the GaN templates at different growth stages with and without from-InGaN-to-GaN interface modification. The growth conditions of the samples are briefly listed in table 1. For the InGaN epilayers without top GaN barriers, samples with and without annealing (∼827 °C, 60 s) were prepared for further comparisons and in-depth analysis of the growth mechanism of the InGaN/GaN SQWs. Without the InGaN-to-GaN interface modification, the InGaN/GaN QWs samples were named as 'A1' for the bare InGaN epilayers without annealing and top barriers, 'A2' for bare InGaN epilayers after annealing and 'A3' with top HT GaN barriers on 'A2'. In comparison, with the interface modification, the InGaN/GaN SQWs and MQWs samples were named as 'B1' for bare InGaN SQW without annealing and top barriers, 'B2' for the bare InGaN SQW after annealing, 'B3' with top HT GaN barriers on 'B2' and 'B4' for the InGaN/GaN MQWs. Another InGaN/GaN SQWs sample ('C3') was also prepared under the same growth conditions as that of sample 'B3' except for growth of the top barrier at low temperature (742 °C) and without annealing during the interface modification process. The other growth conditions for the InGaN/GaN QWs remained the same for all samples. The deposition temperature for the quantum wells and the barriers was 742 °C and 827 °C, respectively. As to the InGaN-to-GaN interface modification, an ultrathin LT GaN layer (about 5–8 Å) was grown prior to the temperature ramping for the growth of HT barrier layers for strain pre-relaxation and suppressing the loss of indium composition, which is important for the growth of high indium content InGaN necessary for the fabrication of green/yellow LEDs. The annealing process

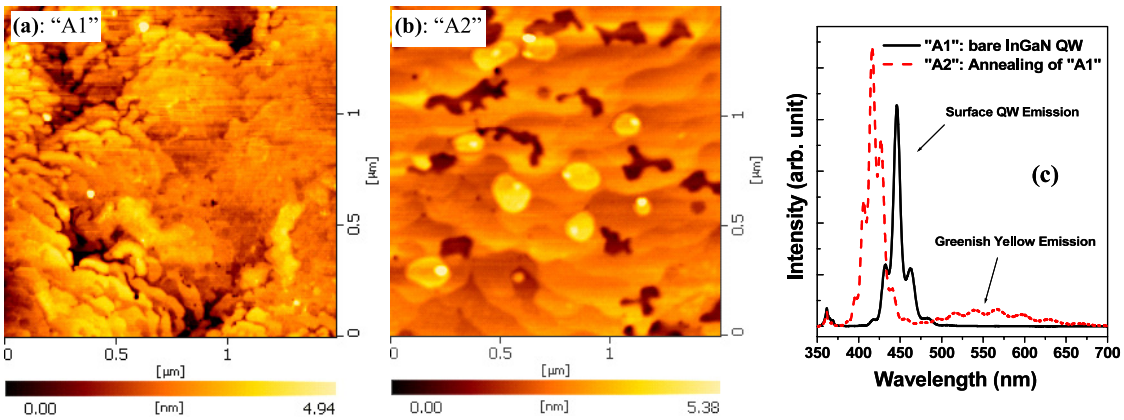

Figure 2. The surface morphology of the InGaN SQW samples without interface modification and top GaN barriers (a) 'A1': before annealing and (b) 'A2': after annealing. (c) The 300 K PL spectra of samples 'A1' and 'A2'.

was employed for elimination/reduction of the indium-rich inclusions and to enhance the two-dimensional (2D) growth of GaN barriers. During the growth of MQWs nitrogen was used as the carrier gas whereas hydrogen was used as the carrier gas at the other growth stages.

The surface morphologies of the InGaN epilayers and InGaN/GaN QWs were investigated by an atomic force microscope (AFM, SPA400, Seiko Instruments Inc.). The surface chemical compositions were analyzed by x-ray photoelectron spectroscopy (XPS, PHI Quantum 2000) with an Al Kα x-ray excitation source ($h\nu$ = 1486.6 eV). The photoluminescence (PL) excited by a 325 nm He–Cd laser was measured at room temperature for the InGaN epilayers and the InGaN/GaN MQWs.

3. Results and discussion

Figure 2(a) shows the surface morphology (1.5 μm × 1.5 μm) of the bare InGaN epilayers on the GaN templates ('A1'). The surface exhibits layer structure with a RMS roughness of 0.7 nm. After annealing (sample 'A2'), as shown in figure 2(b), the surface morphology drastically changed. Lots of surface pits and indium-rich nanoislands were formed on the surface, caused by strain-induced phase separation and indium segregation of the InGaN epilayers during the temperature ramping and annealing at high temperature. The average island size, height and density is about 110 nm, 1.1 nm and 6×10^8cm^{-2}, respectively. The average size, depth and density of pits is about 130 nm, 2.1 nm and 1×10^9 cm^{-2}, respectively. During each successive GaN barrier growth on InGaN well layers, nucleation of new inclusions at the InGaN-to-GaN interface and the continuous growth of previously nucleated inclusions would suppress the barrier growth in a two-dimensional (2D) growth mode and thus result in more defective surfaces. In particular, for the surface characterized as lots of large surface nanoislands and pits, the large and deep surface pits would develop and populate during subsequent growth of HT GaN barriers, progressively deteriorate the surface morphology and form high-density surface pits, which is deleterious for the growth of high-quality MQW structures and fabrication of high-performance LEDs.

The 300 K PL spectra of samples 'A1' and 'A2' have also been measured and shown in figure 2(c). In comparison with the weak band-edge emission (BE) at 361 nm, strong QW emission at 446 nm and 417 nm was observed for samples 'A1' and 'A2', respectively. A strong blueshift of the QW emission by ∼30 nm was observed, indicating the significant loss of the surface indium component. In addition to the normal QW emission, a new peak at ∼550 nm was observed for the annealed sample 'A2'. The origin is likely related to the annealing-induced formation of indium-rich InGaN nanostructures, which will be further discussed later.

In figure 3(a) we show the surface morphology of sample 'B1'—the InGaN epilayers covered by an ultrathin LT GaN layer. Low-temperature growth employed for the ultrathin GaN layers leads to a poor diffusion of Ga atoms which would impede the 2D growth of GaN layers. Further, significant strain would be induced for GaN growth on InGaN due to the lattice mismatch between InN and GaN. As a result of strain pre-relaxation, many nanoislands were newly formed on the smooth surface with an RMS roughness of only 0.3 nm. The island size, height and density is about 20 nm, 1.1 nm and 2×10^9 cm^{-2}, respectively. Generally, strain relaxation would proceed during annealing and growth of HT GaN barriers. In our studies by deposition of the ultrathin LT GaN layers prior to the annealing process and growth of HT GaN barriers, quasi-dots were formed for strain pre-relaxation, which was expected to significantly influence the subsequent growth behavior of HT GaN barriers. As shown in figure 3(b), the commonly observed annealing-induced phase separation of InGaN alloys and formation of large and deep pits (see figure 2(b) for sample 'A2') were greatly suppressed for sample 'B2'. Small and 'thin' surface nanoislands and pits of lower density were observed. Accordingly, the subsequent 2D growth of the HT GaN barrier would not be severely deteriorated due to the absence of large surface pits and indium-rich inclusions. Small indium-rich embedded inclusions were formed inside the pits due to the preferential nucleation of indium-rich clusters under the strain field of the dislocation core (figure 3(b)). The size, height and density of the indium-rich inclusions are about 15 nm, 1.7 nm and 2×10^8 cm^{-2}, respectively; the pit size, depth and density were reduced to about 80 nm, 2.0 nm and

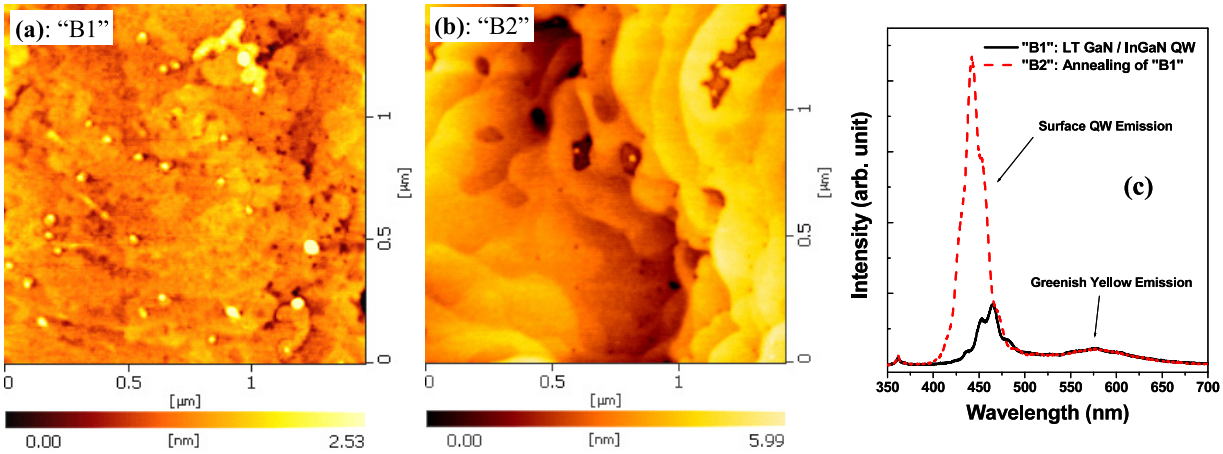

Figure 3. The surface morphology of the interface-modified InGaN SQW samples without top GaN barriers (a) 'B1': before annealing; and (b) 'B2': after annealing. (c) The 300 K PL spectra of samples 'B1' and 'B2'.

7×10^8 cm^{-2}, respectively; a typical layer structure was clearly observed. The appearance of layer structure, absence of indium-rich nanoislands and reduction of pit density definitely indicated improvement of surface smoothness and InGaN/GaN surface/interface qualities, which are highly desirable for the growth of high-quality MQW structures and high-performance LEDs.

Figure 3(c) shows the 300 K PL spectra of samples 'B1' and 'B2'. In comparison with the very weak BE at 361 nm, strong QW emission at about 465 (444) nm was observed for sample 'B1' ('B2'). After annealing the QW emission was significantly enhanced by about five times, indicating the improvement of surface/interface qualities and the formation of effective surface quantum wells. Further, the ultrathin LT GaN layers seemed to be able to prevent/reduce the loss of indium composition as inferred from the smaller blueshift of the QW emission (∼20 nm) than that of 'A2' (∼30 nm), which will be further confirmed by XPS results. In addition to the BE and QW emission, a greenish yellow peak was observed at about 550 nm for samples 'A2', 'B1' and 'B2'. As we can see from the surface morphology of these samples (see figures 2(b), 3(a) and (b)), a common feature is the presence of indium-rich InGaN nanostructures. The energy band structures, characterized as an InGaN/GaN SQW of a high-energy bandgap and the indium-rich nanostructures of a low-energy bandgap, are sketched in figure 4 for interpretation of the double PL peaks corresponding to the normal QW blue emission and the greenish yellow emission. Recently layer structures composed of both InGaN/GaN QWs and indium-rich InGaN nanostructures have been applied in fabrication of cool-white phosphor-free white LEDs [35]. However, the indium-rich InGaN nanostructures would probably increase the pit density and deteriorate the surface smoothness necessary for the subsequent growth of high-quality InGaN/GaN MQWs.

To further examine the influences of interface modification (both coverage of ultrathin LT GaN layers and annealing) on the surface compositions, especially for the indium and gallium compositions, XPS spectra (after background subtraction and intensity normalization to the Ga 2p3 peak) of the Ga 2p3 and

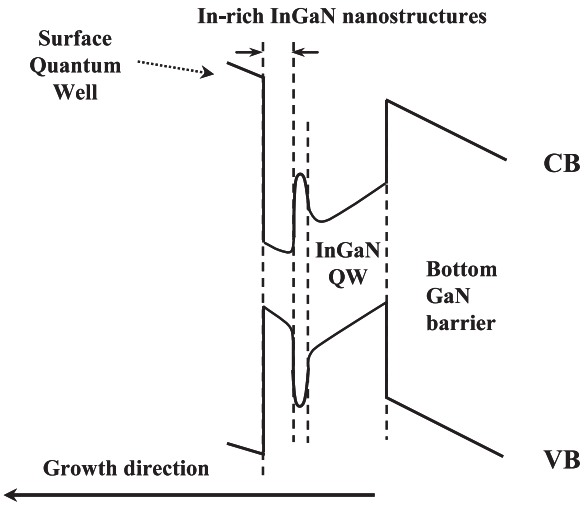

Figure 4. Schematic diagram for the band structures of the InGaN/GaN SQW and indium-rich InGaN nanostructures.

In 3d photoelectron peaks for samples 'A1', 'A2', 'B1' and 'B2' were investigated and shown in figure 5. The Ga 2p3 peak is located at around 1117.1 eV (Ga) whereas the In 3d5 peak is at 444.8 eV. Slight variation of the peak position was observed due to changes in the chemical environment. The percentage of indium composition in the sum of indium and gallium can be estimated by $X_{\mathrm{In}} = \frac{I_{\mathrm{In\ 3d5}}/F_{\mathrm{In\ 3d5}}}{(I_{\mathrm{In\ 3d5}}/F_{\mathrm{In\ 3d5}}+I_{\mathrm{Ga\ 2p3}}/F_{\mathrm{Ga\ 2p3}})}$, where I denotes the integrated intensity of the XPS photoelectron peaks and F the sensitivity factors ($F_{\mathrm{Ga\ 2p3}} = 2.751$ and $F_{\mathrm{In\ 3d5=4.53}}$). As a result we get $X_{\mathrm{In}}^{\mathrm{A1}} \approx 15.8\%$, $X_{\mathrm{In}}^{\mathrm{B1}} \approx 10.4\%$, $X_{\mathrm{In}}^{\mathrm{A2}} \approx 3.0\%$ and $X_{\mathrm{In}}^{\mathrm{B2}} \approx 4.2\%$, respectively. The surface indium content of sample 'B1' (10.4%) is below than that of sample 'A1' (15.8%), indicating the partial coverage of the InGaN well layers by the ultrathin LT GaN layers. After annealing, the outermost surface indium content substantially decreased from 15.8% (10.4%) for 'A1' ('B1') to 3.0% (4.2%) for 'A2' ('B2'), indicating the loss of indium component at the outermost surface and suggesting the formation of surface quantum wells with top InGaN layers of less indium content as a top barrier.

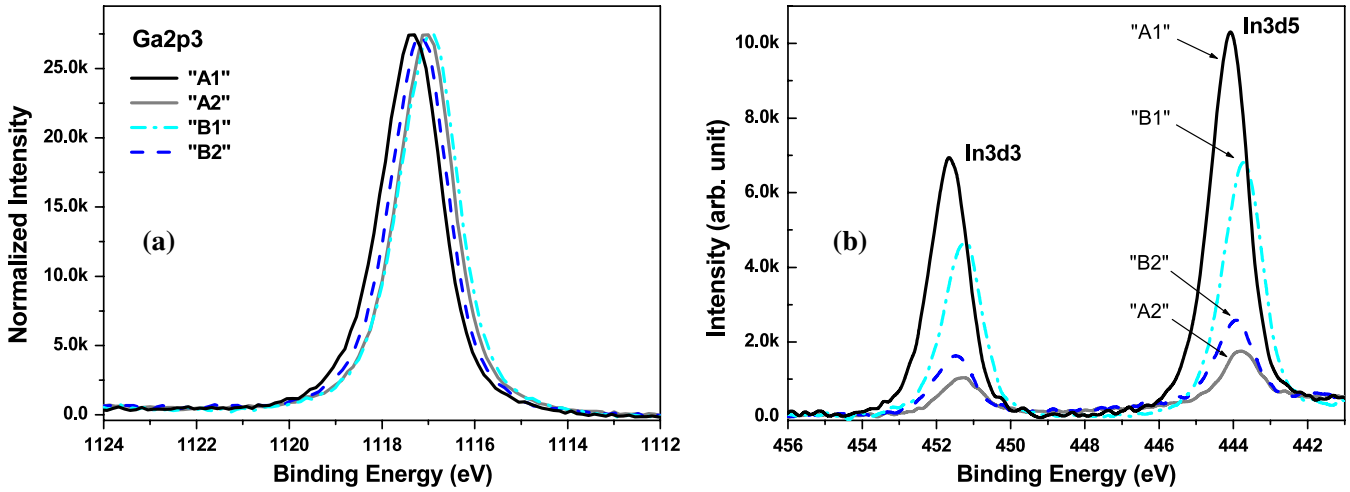

Figure 5. XPS spectra of samples 'A1', 'A2', 'B1' and 'B2': (a) the normalized Ga 2p3 photoelectron peak and (b) the In 3d photoelectron peak.

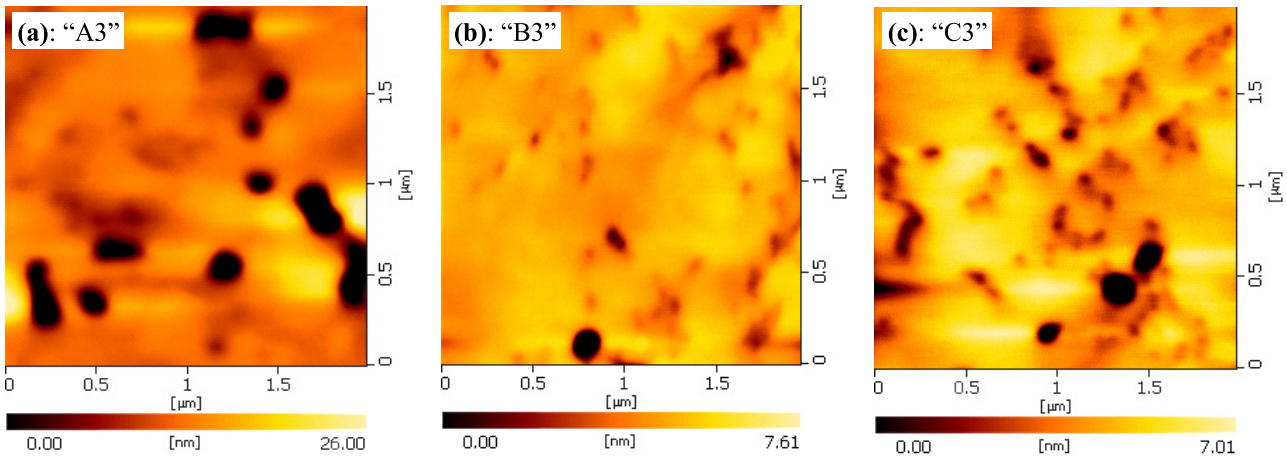

Figure 6. The surface morphology of the InGaN/GaN SQWs on GaN templates with top barriers (a) grown at high temperature (827 °C) without interface modification (sample 'A3'); (b) grown at high temperature (827 °C) with interface modification (sample 'B3'); and (c) grown at low temperature (742 °C) without annealing of the InGaN epilayers prior to the growth of the LT GaN barriers (sample 'C3').

Interestingly, while the indium content of 'B1' (10.4%) is less than that of 'A1' (15.8%), after the same annealing process, the indium content of 'B2' (4.2%) becomes larger than that of 'A2' (3.0%). This suggested that the interface modification by insertion of the ultrathin LT GaN layers between the InGaN well layers and the HT GaN barriers may possess a good protection property for reducing the loss of indium content of InGaN well layers. This is also consistent with the previous PL results, i.e. less blueshift of the QW emission peak for sample 'B2' compared with that of sample 'A2'.

Figure 6 shows the surface morphology (2.0 μm $\times$ 2.0 μm) of samples 'A3' and 'B3', i.e. the InGaN/GaN SQWs with top GaN barriers on samples 'A2' and 'B2', respectively. For the sample without interface modification ('A3'), the surface became quite rough after the subsequent growth of GaN barriers (figure 6(a)). Many large and deep pits were observed on the surface with an RMS roughness, average pit size, depth and density of 4.7 nm, 170 nm, 20 nm and 7×10^8 cm^{-2}, respectively. During the growth of the GaN barriers, the continuous growth of the previously nucleated embedded inclusions, indium-rich InGaN nanoislands and large surface pits of sample 'A2' suppressed the recovery of 2D GaN growth at high temperature and accounted for the more defective morphology. In comparison, with interface modification, the surface was smooth with an RMS roughness of as small as 0.9 nm (sample 'B3'), indicating a fast recovery of 2D GaN growth at high temperature due to the strain pre-relief-induced suppression of phase separation. The average pit size, depth and density is about 70 nm, 4.0 nm and 8×10^8 cm^{-2}, respectively. For further comparisons, sample 'C3' was prepared with GaN barriers grown at low temperature (742 °C) and a lack of the annealing process of the InGaN well layers. All the other growth conditions are the same as that of sample 'B3'. The RMS roughness, average pit size, depth and density of sample 'C3' are about 1.6 nm, 80 nm, 4.5 nm and 2×10^9 cm^{-2}, respectively. Apparently, as shown in figure 6(c), the surface is featured as smaller and shallower surface pits but with higher pit density in comparison with that

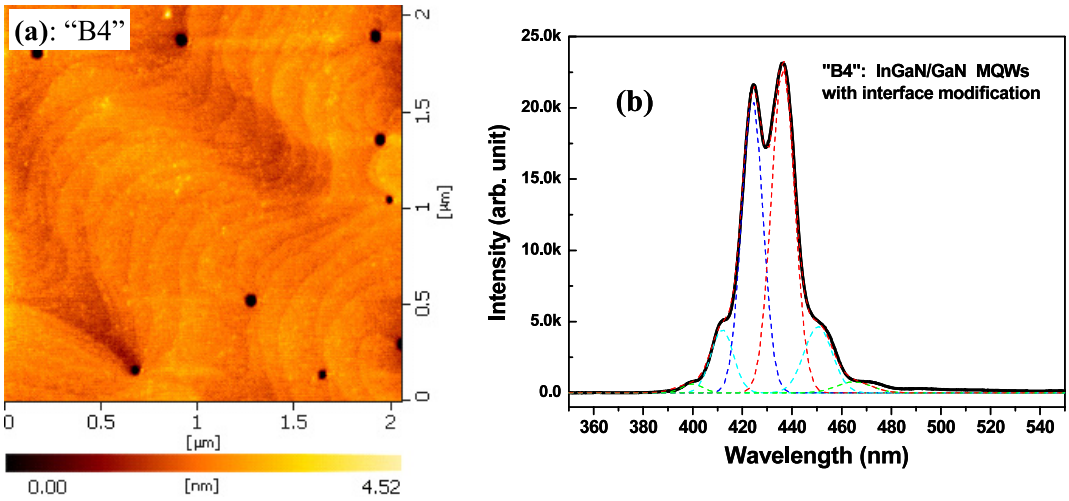

Figure 7. (a) The surface morphology and (b) 300 K PL spectra of the interface modified InGaN/GaN MQWs (sample 'B4').

of sample 'A3'. With interface modification for sample 'B3' the surface/interface quality is greatly improved with very good smoothness and relatively low pit density; further, the surface pits of sample 'B3' are smaller and shallower compared with that of sample 'A3' indicating the improvement of the interface abruptness. The improvement of the interface smoothness of the InGaN/GaN SQWs is very important for the subsequent growth of high-quality MQW structures and fabrication of high-performance LEDs with good control of doping and layer structures.

Following sample 'B3' with improvement of the surface/interface qualities and enhancement of the optical property, an InGaN/GaN MQW (sample 'B4') has also been prepared with the same interface modification technique in each successive InGaN/GaN SQW as that of sample 'B3'. As shown in figure 7(a), the sample surface is very smooth with an RMS roughness of only 0.4 nm. The layer structure is evident, indicating the enhanced 2D growth of the subsequent HT GaN barrier. The surface pit size, depth and density is about 60 nm, 4.8 nm and 2×10^8 cm^{-2}, respectively. The decrease in pit density and elimination of the indium-rich nanostructures suggest that the enhanced 2D barrier growth might suppress the nucleation of the indium-rich clusters and further growth of the inclusions and pits. As shown in figure 7(b), a very strong MQW emission peak at ∼432 nm was observed whereas the GaN BE emission becomes invisible. The disappearance of the long-wavelength emission peak corresponding to the indium-rich nanostructures suggests elimination of the indium-rich nanostructures and enhancement of the normal MQW emission. Further, the observation of Fabry–Perot interference fringes indicates a smooth surface/interface being formed, which is also consistent with the AFM results. As the MQWs growth was significantly influenced by the bottom QW, growth of high-quality SQWs becomes very important. As observed by AFM and PL measurements, the MQWs which consist of five periods of interface-modified SQWs possess good surface/interface qualities and optical properties, indicating an improvement of the SQW as well as MQWs by the interface modification.

4. Conclusion

An interface modification technique was employed to improve the properties of the InGaN/GaN QWs. By insertion of an ultrathin LT GaN layer (about 5–8 Å) between the InGaN wells and the HT GaN barriers followed by an annealing process, the growth behavior of the InGaN/GaN QWs was greatly influenced. An ultrathin LT GaN layer was employed to avoid the generation of high-density defects. The subsequent annealing process was employed for the reduction of newly formed defects. The morphology changes of the InGaN/GaN QWs at different growth stages with and without the interface modification were studied in detail. We find that the InGaN alloy phenomena such as indium aggregation and phase separation, generally caused by annealing during the subsequent growth of HT GaN barriers, were suppressed due to the strain pre-relaxation by formation of nanoislands on the InGaN wells during the coverage of the ultrathin LT GaN layers prior to the temperature ramping. As investigated by AFM, the surface/interface qualities were significantly improved with better surface smoothness, and smaller and shallower V-defects of lower density for the samples with interface modification compared with that without modification. Further, XPS was employed to investigate the surface compositions of the bare and interface-modified InGaN QWs before and after annealing, which revealed the good protection property of the ultrathin LT GaN layers as observed by PL measurements.

Acknowledgment

This work was partially supported by the National Natural Science Foundation of China under grant no. 60876008.

References

[1] Yam F K and Hassan Z 2008 *Superlatt. Microstruct.* **43** 1
[2] Oliver R A, Kappers M J, Humphreys C J and Briggs G A D 2005 *J. Appl. Phys.* **97** 013707

[3] Suihkonen S, Lang T, Svensk O, Sormunen J, Törmä P T, Sopanen M, Lipsanen H, Odnoblyudov M A and Bougrov V E 2007 *J. Cryst. Growth* **300** 324
[4] Ponce F A and Bour D P 1997 *Nature* **386** 351
[5] Nakamura S 1998 *Science* **281** 956
[6] Orton J W and Foxon C T 1998 *Rep. Prog. Phys.* **61** 1
[7] Ryu H Y *et al* 2007 *IEEE Photon. Technol. Lett.* **19** 1717
[8] Schubert E F and Kim J Y 2005 *Science* **308** 1274
[9] Krames M R *et al* 2002 *Phys. Status Solidi* a **192** 237
[10] Nizamoglu S and Demir H V 2007 *Nanotechnology* **18** 405702
[11] Soh C B, Chow S Y, Tripathy S and Chua S J 2008 *J. Phys.: Condens. Matter* **20** 095210
[12] Niu N H, Wang H B, Liu J P, Liu N X, Xing Y H, Han J, Deng J and Shen G D 2006 *J. Cryst. Growth* **286** 209
[13] Johnson M C, Bourret-Courchesne E D, Wu J, Liliental-Weber Z, Zakharov D N, Jorgenson R J, Ng T B, McCready D E and Williams J R 2004 *J. Appl. Phys.* **96** 1381
[14] Cheng Y C, Wu C M, Chen M K, Yang C C, Feng Z C, Li G A, Yang J R, Rosenauer A and Ma K J 2004 *Appl. Phys. Lett.* **84** 5422
[15] Liu W, Chua S J, Zhang X H and Zhang J 2003 *Appl. Phys. Lett.* **83** 914
[16] Huang C F, Tang T Y, Huang J J, Shiao W Y, Yang C C, Hsu C W and Chen L C 2006 *Appl. Phys. Lett.* **89** 051913
[17] Park J S, Moon Y T, Kim D J, Park N M, Yao T and Park S J 2008 *J. Phys. D: Appl. Phys.* **41** 165103
[18] Huang C F, Liu T C, Lu Y C, Shiao W Y, Chen Y S, Wang J K, Lu C F and Yang C C 2008 *J. Appl. Phys.* **104** 123106
[19] Kumar M S, Lee Y S, Park J Y, Chung S J, Hong C H and Suh E K 2009 *Mater. Chem. Phys.* **113** 192
[20] Lai W C, Huang Y S, Yen Y W, Sheu J K, Hsueh T H, Kuo C H and Chang S J 2008 *Phys. Status Solidi* c **5** 1639
[21] Lin H C, Lin R S and Chyi J I 2008 *Appl. Phys. Lett.* **92** 161113
[22] Kumar M S, Park J Y, Lee Y S, Chung S J, Hong C H and Suh E K 2008 *Japan. J. Appl. Phys.* **47** 839
[23] Fang Z L, Kang J Y and Shen W Z 2009 *Nanotechnology* **20** 045401
[24] Ju J W, Kim H S, Jang L W, Baek J H, Shin D C and Lee I H 2007 *Nanotechnology* **18** 295402
[25] Leem S J, Shin Y C, Kim E H, Kim C M, Lee B G, Moon Y B, Lee I H and Kim T G 2008 *Semicond. Sci. Technol.* **23** 125039
[26] Pendlebury S T, Parbrook P J, Mowbray D J, Wood D A and Lee K B 2007 *J. Cryst. Growth* **307** 363
[27] Ju J W, Kang E S, Kim H S, Jang L W, Ahn H K, Jeon J W, Lee I H and Baek J H 2007 *J. Appl. Phys.* **102** 053519
[28] Florescu D I, Ting S M, Ramer J C, Lee D S, Merai V N, Parkeh A, Lu D, Armour E A and Chernyak L 2003 *Appl. Phys. Lett.* **83** 33
[29] Suihkonen S, Svensk O, Lang T, Lipsanen H, Odnoblyudov M A and Bougrov V E 2007 *J. Cryst. Growth* **298** 740
[30] Scholz F, Off J, Fehrenbacher E, Gfrorer O and Brockt G 2000 *Phys. Status Solidi* a **180** 315
[31] Ting S M *et al* 2003 *J. Appl. Phys.* **94** 1461
[32] Moon Y T, Kim D J, Song K M, Choi C J, Han S H, Seong T Y and Park S J 2001 *J. Appl. Phys.* **89** 6514
[33] Fang Z L, Li S P, Li J C, Sun H Z, Wang S J and Kang J Y 2008 *Thin Solid Films* **516** 6344
[34] Fang Z L, Kang J Y and Shen W Z 2008 *J. Phys. Chem.* C **112** 17652
[35] Soh C B, Liu W, Teng J H, Chow S Y, Ang S S and Chua S J 2008 *Appl. Phys. Lett.* **92** 261909